

# Nanophotonic Devices for Optical Interconnect

Dries Van Thourhout, *Member, IEEE*, Thijs Spuesens, *Member, IEEE*, Shankar Kumar Selvaraja, *Student Member, IEEE*, Liu Liu, Günther Roelkens, *Member, IEEE*, Rajesh Kumar, Geert Morthier, *Senior Member, IEEE*, Pedro Rojo-Romeo, *Member, IEEE*, Fabien Mandorlo, Philippe Regreny, Oded Raz, *Member, IEEE*, Christophe Kopp, and Laurent Grenouillet

(Invited Paper)

**Abstract**—We review recent progress in nanophotonic devices for compact optical interconnect networks. We focus on microdisk-laser-based transmitters and discuss improved design and advanced functionality including all-optical wavelength conversion and flip-flops. Next we discuss the fabrication uniformity of the passive routing circuits and their thermal tuning. Finally, we discuss the performance of a wavelength selective detector.

**Index Terms**—Flip-flop, heterogeneous integration, microdisk laser (MDL), network-on-chip, photonic integration, process uniformity, silicon-on-insulator (SOI), wavelength conversion.

## I. INTRODUCTION

WITH the required data rates, ever increasing optical communication is coming closer and closer to the chip. To be a valid alternative for electrical communication, the optical link has to provide at least the same bandwidth as current copper solutions at lower cost and with improved density. Current short-reach optical interconnect solutions are mostly based on multimode fibers and/or waveguides in combination with vertical cavity surface-emitting laser (VCSELs) [1], [2]. However, these do not provide a long-term solution for the bandwidth density problem. The line rates are limited and the currently

proposed systems often require costly assembly techniques because they are not compatible with wafer scale fabrication.

Silicon photonics potentially could provide optical links, which are scalable in bandwidth, e.g., by using wavelength-division multiplexing (WDM), which are compatible with wafer scale fabrication and testing. Recently, it was shown by several groups that it is possible to fabricate very compact optical waveguide circuits using the same type of equipment and tools as those used for fabricating the most advanced electronic integrated circuits [3]–[5]. The waveguides are fabricated starting from a silicon-on-insulator (SOI) substrate with a 200–250 nm-thick silicon top layer on which the devices are patterned using either electron beam lithography or deep UV (DUV) lithography. Subsequently, the waveguides are defined using reactive ion etching. Due to the high index contrast, a very small bend radius can be used (0.01 dB/90° loss for a 5 μm bend and 0.04 dB/90° loss for a 2 μm bend). However, also because of the high index contrast, even the smallest remaining sidewall roughness—published values range from 1 to 3 nm—gives rise to considerable propagation losses (1–3 dB/cm). However, due to the compactness of the devices, the propagation loss often has only a minor impact on their overall performance. Several groups now also demonstrated active devices, such as modulators [6]–[8] and high-speed photodetectors integrated with such waveguide circuits [9]. When using an off-chip source, these devices in principle provide sufficient functionality for building data links [10] or even more complex optical networks [11]–[13]. Though, further improvement in power consumption and size of these components is still required [14].

However, for complex optical networks, using an off-chip optical source becomes increasingly difficult. The circuits required for distributing the optical feed may induce considerable loss, consume an important fraction of the available space and are difficult to design. Therefore, we investigated the possibility for integrating compact microsources directly on top of the electronic circuits. The requirements for these microsources are very stringent. They should have low power consumption and compact footprint, they should be electrically injected and compatible with direct modulation at 5 to 10 Gb/s, and they should couple the light efficiently to the silicon optical waveguide layer. In addition, they should be compatible with wafer scale fabrication technologies. In Section II of this paper, we describe the microdisk laser (MDL) we developed for this purpose and its basic properties (threshold, spectrum, and direct modulation). In Section III, we describe some advanced properties, which may be necessary for scaling up wavelength-routed networks [15],

Manuscript received October 7, 2009; revised December 24, 2009; accepted January 6, 2010. Date of publication March 4, 2010; date of current version October 6, 2010. This work was supported by the European Commission under Project ICT-WADIMOS and Project ICT-HISTORIC under the 7th Framework Programme (FP7), Information and Communications Technologies (ICT).

D. Van Thourhout, T. Spuesens, S. K. Selvaraja, G. Roelkens, R. Kumar, and G. Morthier are with the Department of Information Technology, Interuniversity Microelectronics Center, Ghent University, Ghent 9000, Belgium (e-mail: dries.vanthourhout@intec.ugent.be).

L. Liu was with the Department of Information Technology, Interuniversity Microelectronics Center, Ghent University, Ghent 9000, Belgium. He is now with the Department of Photonics Engineering, Technical University of Denmark, DK-2800 Lyngby, Denmark.

P. Rojo-Romeo and P. Regreny are with the Institut des Nanotechnologies de Lyon (INL), INL-Unité Mixte de Recherche (UMR) 5270, Centre National de la Recherche Scientifique (CNRS), Ecole Centrale de Lyon, Université de Lyon, F-69134 Lyon, France.

F. Mandorlo is with the Institut des Nanotechnologies de Lyon (INL), INL-Unité Mixte de Recherche (UMR) 5270, Centre National de la Recherche Scientifique (CNRS), Ecole Centrale de Lyon, Université de Lyon, F-69134 Lyon, France, and also with the Commissariat à l’Energie Atomique-Laboratoire d’Electronique de Technologie de l’Information (CEA-LETI), Minattec, 308054 Grenoble, France.

O. Raz is with the Eindhoven University of Technology, 5612 Eindhoven, The Netherlands.

C. Kopp and L. Grenouillet are with the Commissariat à l’Energie Atomique-Laboratoire d’Electronique de Technologie de l’Information (CEA-LETI), Minattec, 308054 Grenoble, France.

Color versions of one or more of the figures in this paper are available online at <http://ieeexplore.ieee.org>.

Digital Object Identifier 10.1109/JSTQE.2010.2040711

such as all-optical wavelength conversion, all-optical gating, and optical bistability. In Section IV, we give some more details on the fabrication and characteristics of the passive waveguide circuits, and in particular, on the fabrication uniformity and tolerances. We also propose integrated thermal tuners, which may help to overcome the device nonuniformity. In Section V, we describe the development of a wavelength selective detector.

## II. MDL-BASED TRANSMITTER

### A. Introduction

Thus far, only compound semiconductor materials with a direct bandgap have shown to exhibit sufficient gain for realizing compact electrically driven microsourses. Unfortunately, due to the large lattice mismatch, monolithic integration with silicon has proven to be difficult. Hybrid integration, whereby prefabricated components are integrated with the waveguides using accurate pick-and-place equipment does allow for prescreening of the lasers, but is not compatible with wafer scale integration, and hence, not suitable for use in combination with very dense optical network circuits [16]–[18]. Therefore, several research groups proposed and demonstrated an alternative integration process based on the use of wafer and/or die bonding [19]–[21]. Thereby, high quality InP-based epitaxial layers are bonded on-top of preprocessed silicon waveguides. Direct bonding processes [22] as well as molecular (silica-to-silica) [23] and adhesive bonding processes have been used [24]. Subsequently, the substrate is removed and the optoelectronic devices are defined collectively using wafer scale processes.

The microsourses we developed were fabricated using this so-called heterogeneous integration process. Because they had proven to be efficient light emitters already using a monolithic integration platform [25], we decided to focus on microdisk type devices. Initial devices were optically pumped [26], [27] or not yet coupled to silicon waveguides [28]. In 2007, we demonstrated for the first time an electrically injected microlaser [29]. Continuous wave (CW) operation could be shown, but the optical output power and external efficiency were still low. Recently, we demonstrated a new generation of devices with improved epitaxial layers and processing scheme, leading to a considerable decrease in threshold current and the demonstration of new functionality, such as bistable operation (see Section III). In the next section, we describe these design improvements in more detail.

### B. Improved MDL Design and Operation

Fig. 1 gives a schematic representation of the heterogeneously integrated MDL. The device was etched in a thin InP-based membrane, which was bonded on top of the silicon waveguides using an adhesive bonding process based on benzocyclobutene (BCB). The silicon waveguide underneath was 500 nm wide and had a thickness of 220 nm (see [30] for details on the fabrication process). The laser mode is evanescently coupled to this waveguide. Careful alignment of the disk with respect to the waveguide is important to achieve a good coupling efficiency (see [31] for details on the disk-waveguide coupling design). Electrical injection is possible via a top metal contact in the

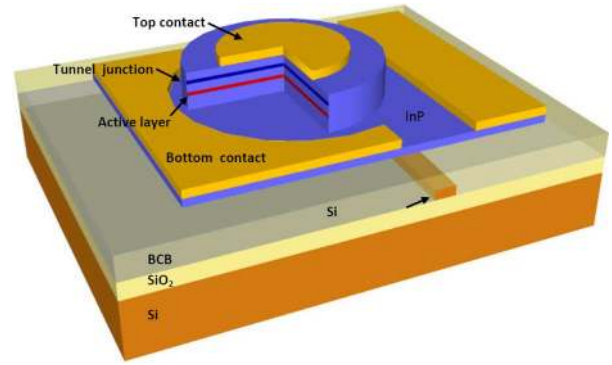


Fig. 1. Schematic representation of a MDL heterogeneously integrated on SOI.

TABLE I  
LAYER STRUCTURE OF IMPROVED MICRODISK DESIGN

<b>N+ (<math>5 \times 10^{18} \text{cm}^{-3}</math> to <math>1 \times 10^{18} \text{cm}^{-3}</math>) InP : 80 nm</b>	} Tunnel junction	} P contact
<b>N++ (<math>1 \times 10^{19} \text{cm}^{-3}</math>) Q1.3 : 25 nm</b>		
<b>P++ (<math>2 \times 10^{19} \text{cm}^{-3}</math>) Q1.3 : 25 nm</b>		
<b>P+ (<math>5 \times 10^{17} \text{cm}^{-3}</math> to <math>1 \times 10^{18} \text{cm}^{-3}</math>) InP : 135 nm</b>		
<b>Q1.2 (nid) Q1.2 : 25 nm</b>		
<b>3 x 6 nm InAsP QWs / 3 x 15 nm Q1.2 barriers</b>		
<b>Q1.2 (nid) Q1.2 : 25 nm</b>		
<b>N (<math>1 \times 10^{18} \text{cm}^{-3}</math>) Q1.2 : 120 nm</b>		
<b>N+ (<math>5 \times 10^{18} \text{cm}^{-3}</math>) InP : 95 nm</b>		} N contact

Note: Structure is grown upside down for compatibility with bonding process.

center of the disk and a bottom contact on a 100-nm-thin lateral contact layer. The details of the layer structure are shown in Table I.

The heterostructures were grown at 490 °C using solid source molecular beam epitaxy (SSMBE) on a two inch InP wafer supplied by InPact S. A. An InGaAs sacrificial etch-stop layer, which is removed following bonding, was grown first. The structure consists, starting from the bottom layer of a 95-nm-thick  $5 \times 10^{18} \text{cm}^{-3}$  Si-doped InP bottom contact layer, a 120-nm-thick InGaAsP quaternary emitting at 1.2  $\mu\text{m}$  (Q1.2)  $1 \times 10^{18} \text{cm}^{-3}$  Si doped n-layer, a 25 nm Q1.2 spacer layer, three 6-nm-thick compressively strained InAsP quantum wells (QWs) embedded in 15 nm Q1.2 barriers, a 25 nm Q1.2 spacer layer, a 135-nm-thick  $5 \times 10^{17}$  to  $1 \times 10^{18} \text{cm}^{-3}$  Be doped InP layer, and the p-type contacts layers. Metal contacts have usually a poor resistivity on p-type InP, and in standard devices, it is necessary to add a p-type InGaAs contact layer to improve the contact resistance. However, this InGaAs layer is highly absorbing around 1.55  $\mu\text{m}$ . To overcome this issue, we replaced the p-contact by a p+/n+ tunnel junction and a n+ contact layer. The top contact

then constitutes of a 20-nm-thick p+ ( $2 \times 10^{19} \text{ cm}^{-3}$ ) InGaAsP emitting at 1.3  $\mu\text{m}$  (Q1.3) layer, a 20-nm-thick n+ ( $1 \times 10^{19} \text{ cm}^{-3}$ ) Q1.3 layer, and finally, a 80 nm n+ ( $5 \times 10^{18}$  to  $1 \times 10^{18} \text{ cm}^{-3}$ ) InP contact layer. This tunnel junction-based contact can be used either as the bottom contact, as was the case in our earlier paper [29] or as the top contact, which is the case here. When used as a bottom contact, the tunnel junction acts as an etch-stop layer during the fabrication of the bottom contact slab. However, in this configuration, the tunnel junction is close to the waveguide below the microdisk and the optical losses due to the high p-doping level increases. Therefore, in our recent work, we reversed the growth order and now the tunnel junction forms the top contact of the device, leading to lower optical confinement, and hence, lower optical losses in this layer.

The new epitaxial structure has a total thickness of 580 nm, which is significantly thinner than the previous structure (955 nm). This has a positive effect on the scattering loss and the coupling efficiency. It can be shown that taking into account the large vertical confinement, the scattering loss, which is caused by the sidewall roughness of the microdisk, scales roughly linearly with the thickness of the device [32]. The coupling efficiency to the underlying waveguide also increases for a thinner structure, because there exists a larger exponential tail in the cladding, and thus, also a larger overlap with the silicon waveguide.

In earlier devices, the low thermal conductivity of the dielectric layers surrounding the microdisk device, including the SOI box layer, the bonding layer, and the passivation layers, resulted in severe self-heating of the device [33]. Therefore, in the current design, we implemented an improved thermal heat sink under the form of a thick layer of gold (600 nm) on the top contact of the microdisk. Although, a thermal roll-over effect is still present, saturation of the output power now occurs around a drive current of 4 mA instead of 2 mA in previous devices.

For these devices, CW lasing at room temperature was observed for microdisks with a diameter of 7.5 and 10  $\mu\text{m}$ . Fiber grating couplers [34] were used to collect the light at one end of the silicon waveguide. The fiber coupled power for a 7.5  $\mu\text{m}$  diameter microdisk, is shown in Fig. 2, together with the voltage–current response. A threshold current of 350  $\mu\text{A}$  and a maximum output power in the fiber of 38  $\mu\text{W}$  was measured. The oscillations in the light output curve are due to reflections of the grating couplers, which are placed at both sides of the output waveguide. The abrupt change in the curve around 2.4 mA is related to a change in the lasing wavelength from 1554 nm to the next fundamental mode with a lower azimuthal mode number at 1584 nm, due to self-heating of the device. Since the output couplers are wavelength dependent, this at least partly explains the jump in the output power. The grating couplers have an efficiency of 21% at 1554 nm and 30% at 1584 nm, which means the maximum power coupled into the waveguide is 120  $\mu\text{W}$ . This is a considerable improvement compared to the previous generation. The optical spectrum when a 4 mA drive current is applied to the microdisk, is shown in Fig. 3. The lasing wavelength is 1584 nm and the fundamental mode has a free spectral range (FSR) of about 30 nm. The side-mode suppression ratio (SMSR) is 35 dB. The power consumption of the device will be dominated by its static drive power, which is

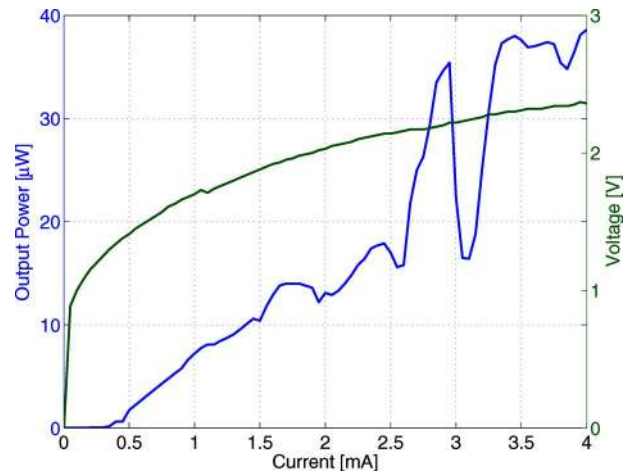


Fig. 2. Output power and voltage vs. current for a 7.5- $\mu\text{m}$  diameter MDL.

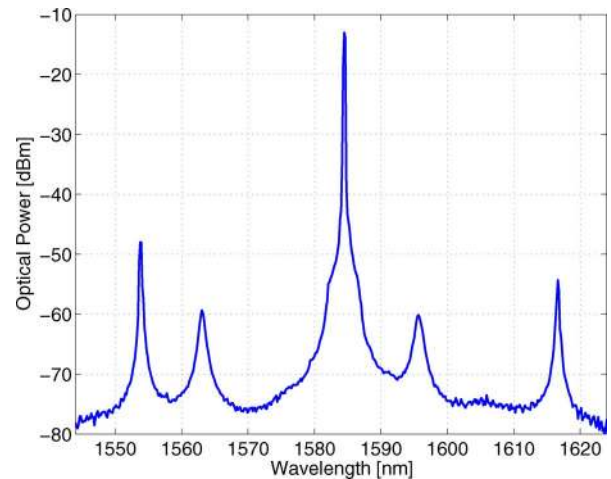


Fig. 3. Optical spectrum of a 7.5- $\mu\text{m}$  diameter microdisk.

about 4 mW at 2 mA drive current. For a 10 Gb/s data stream, this leads to a power consumption of 400 fJ/b, not including the dynamic part of the power consumption and the consumption in the driver circuits. Hence, further improvements are needed to reach the 100 fJ/b target [14]. These could include single-sided emission, reduced injection in center of disk, smaller disk radius, and improved processing.

### C. Multiwavelength Transmitter

As discussed already in Section I of this paper, WDM technology is essential for scaling up the communication capacity of a single link. Wavelength information can also be used to improve the functionality of an optical interconnect network, e.g., to control the routing of the communication signals toward the different cores within the network. For these applications a multiwavelength laser (MWL) source, which can emit several wavelength signals, preferably at a predefined channel grid is required. Such a laser can be implemented straightforwardly by cascading several MDLs on a single silicon bus waveguide, as shown in Fig. 4(a) [1]. Fig. 4(b) and c shows the measured spectra of two 4-channel MWLs: one with 6 nm channel spacing,

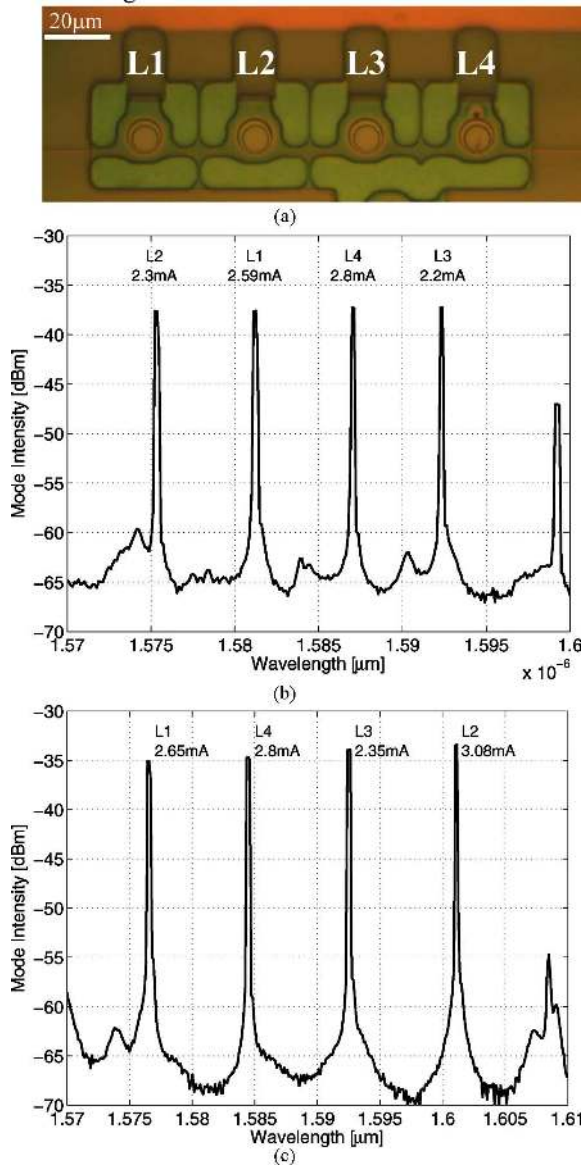


Fig. 4. (a) Fabricated MWL before metallization, composed of four MDLs on a single silicon bus waveguide. (b) and (c) Spectra of MWLs with 6 and 8 nm channel spacing. The bias current of each MDL and the laser number is indicated on the corresponding lasing peak [35].

and the other with 8 nm channel spacing. The bias currents of the MDLs have been adjusted individually, in order to achieve a uniform power for all channels. Due to the fabrication accuracy, the lasing wavelengths of identical microdisks vary about  $\pm 500$  pm within the same chip. Therefore, wavelength trimming, e.g., through the thermo-optical effect by implementing a local heater, is needed to align each of the lasing peaks to the designed channel grid. A possible implementation is discussed in the following section.

#### D. Dynamic Response of MDL

The dynamic response of an MDL was tested by directly modulating the bias current using first generation devices (having limited output power). Fig. 5 shows the response of a  $7.5 \mu\text{m}$

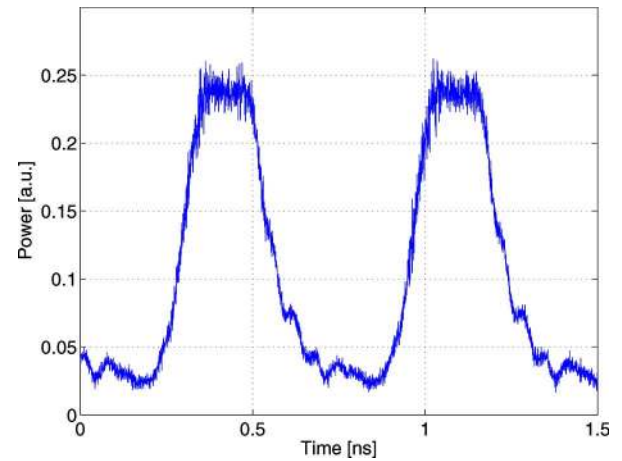


Fig. 5. Direct current modulation response of a  $7.5\text{-}\mu\text{m}$  diameter MDL with an electrical driving signal of a periodic square-wave at 1.5 GHz [36].

diameter MDL modulated with a periodic square-wave signal at 1.5 GHz. The low level of the drive signal was slightly above threshold, the high level was at the current giving the highest power. The extinction ratio of the output laser signal is approximately 10 dB after the amplification by an Er-doped fiber amplifier (EDFA). The rise and fall times are 110 and 150 ps, respectively. Due to the low output power ( $2 \mu\text{W}$  coupled to fiber), eye diagrams nor bit error rate could not be measured reliably at this stage. It is believed that the data transmission performance will be improved using a MDL with the improved design as discussed earlier where over  $30 \mu\text{W}$  was measured in fiber.

#### E. Tuning of MDL Wavelength

For tuning the lasing wavelength, we propose a MDL design with an integrated heater, as shown in Fig. 6(a). The heater (which is fabricated in the same III-V layers also used for the disk) is a ring sitting around the microdisk cavity, where the laser field is confined. Fig. 6(b) shows an SEM-picture of the structure immediately following the III-V etching step. The gap between the ring and the central disk is a critical parameter, and should both be small enough to allow for efficient heating and large enough to avoid leakage of the cavity whispering gallery mode to the heater. Simulation suggests that  $1.0\text{--}2.0 \mu\text{m}$  is an optimal value. Fig. 6(c) shows the calculated temperature field distribution when the diameter of the disk is  $7.5 \mu\text{m}$  and the gap is  $1.6 \mu\text{m}$ . The heating efficiency determined at the edge of the central disk is about  $3.4 \text{ K/mW}$ , corresponding to a tuning rate of  $0.34 \text{ nm/mW}$ .

Fig. 7 shows the lasing spectra from the MDL with different electrical powers applied to the integrated heater. The laser driving current was fixed at 1.5 mA. The tuning rate was measured to be  $0.31 \text{ nm/mW}$ , close to the simulated result. A 2.2-nm shift without severe impact on the lasing power could be demonstrated. Larger tuning is possible by applying a higher current to the heater, but comes at the expense of decreasing laser output power.

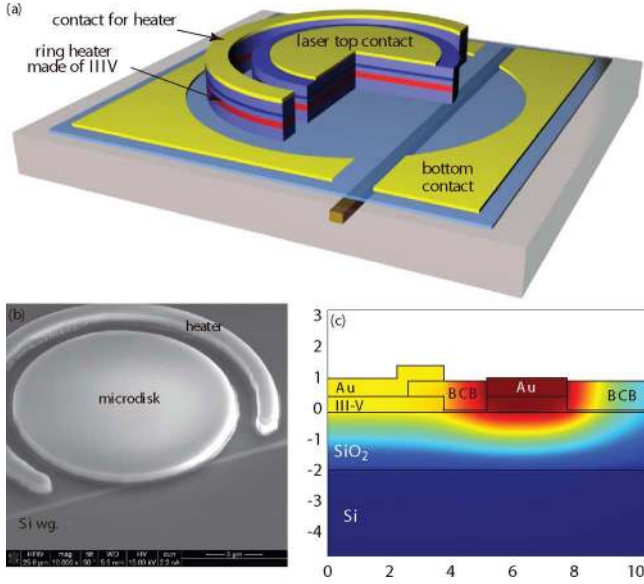


Fig. 6. (a) Sketch of the MDL with an integrated ring heater consisting of a forward-biased III-V p-i-n junction. (b) SEM picture of the microdisk cavity and ring heater. (c) Temperature distribution in the proposed device.

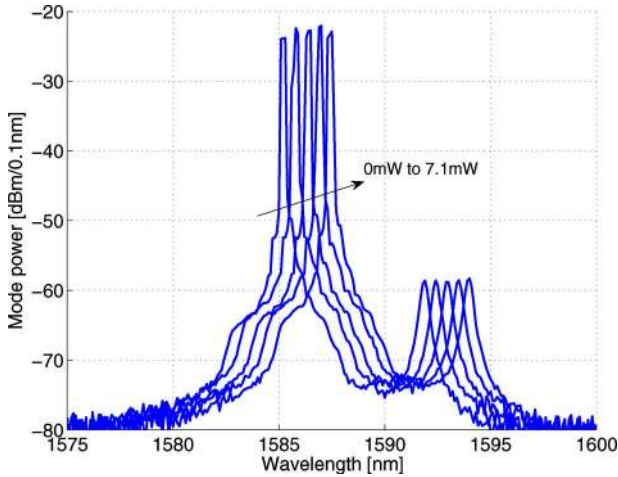


Fig. 7. Tuning of the MDL wavelength. Along the arrow direction, the powers applied to the integrated heater are 0, 1.6, 3.5, 5.3, and 7.1 mW, respectively.

#### F. Design of Microdisk With External Cavity

The modes in the standard MDL can be labeled by a set of numbers  $(l, m, n)$  denoting the radial ( $l$ ), azimuthal ( $m$ ), and vertical ( $n$ ) mode number [37]. By careful design of the metal top contact and the position of the gain layer the modes  $(0, m, 0)$  will have a considerable lower intrinsic loss rate  $\tau_0^{-1}$ , compared to the higher order modes with nonzero  $l$  and  $n$  numbers and will have a much lower threshold gain [31]. However, there is no clear mechanism to select the azimuthal mode number  $m$ . For microdisks with radius larger than  $2 \mu\text{m}$ , the FSR will typically be smaller than the gain bandwidth and lasing in multiple orders may occur. In addition, both clockwise and counter clockwise lasing may occur, which may be undesirable in practical applications or result in decreased usable output power. To resolve these issues, we propose a new configuration, as shown in Fig. 8.

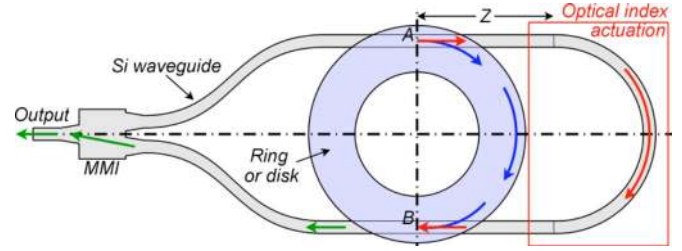


Fig. 8. Microdisk coupled to an outer loop, with a single optical output.

At one side, the microdisk is coupled to an external cavity in the silicon waveguide layer. At the other side, the two outputs are coupled together using e.g., a multimode interference coupler (MMI).

Then, using coupled-mode theory [38], we can demonstrate that the phase difference  $\Delta\varphi_{AB}$  between the two possible optical paths going from A to B, where both controls the resonance frequency  $\omega$  and the  $Q$  of the lasing mode

$$\begin{cases} \omega = \omega_0 - (1/2)A_g\tau_c^{-1}\sin(\Delta\varphi_{AB}) \\ Q = \frac{\tau_0^{-1}}{\tau_0^{-1} + \tau_c^{-1}(1 + A_g\cos(\Delta\varphi_{AB}))} \end{cases} \quad (1)$$

Hereby,  $A_g$  is defined such that  $(1 - A_g)$  represents the relative amplitude attenuation for the mode propagating in the passive waveguide path connecting points A and B.  $\omega_0$  is the resonance frequency of the cavity without the external racetrack. The coupling rate between the disk and a single waveguide is given by  $\tau_c$  and  $\tau_0$ , determines the intrinsic cavity lifetime. By controlling the relative phase difference  $\Delta\varphi_{AB}$  and for low losses in the waveguide, we now can:

- 1) vary the  $Q$  between the values for a standard microdisk coupled to two waveguides without feedback ( $\approx (1/2)Q_c = (1/2)\tau_c\omega$  for constructive interference) and the intrinsic quality factor  $Q_0 = \tau_0\omega$  (for destructive interference);
- 2) adjust the resonance frequency  $\omega$  by  $\pm(\tau_c^{-1}/2)$ .

Fig. 9 shows the evolution of the  $Q$ -factor as a function of the external waveguide length  $Z$  (which controls the phase difference  $\Delta\varphi_{AB}$ ) for five modes with increasing azimuthal mode number  $n$  of a  $4\text{-}\mu\text{m}$  radius microdisk. Depending on the external waveguide length  $Z$ , we denote a different overall behavior. For specific sizes of the external loop [e.g., a few micrometer in Fig. 9(a)], the modes are regularly distributed. Then, by controlling the refractive index of the material, e.g., thermally or through carrier injection, we can fine tune the resonant wavelength, e.g., to compensate small fabrication variations, while still maintaining a high contrast in  $Q$ -factor between the different azimuthal modes, and hence, ensuring single mode operation. In the case of Fig. 9(b), the odd modes and even modes, each almost share the same phase condition. The frequency separation between two modes with high  $Q$ -factor is doubled, resulting in a doubling of the practical FSR, and hence, higher SMSR. In Fig. 9(c), all modes almost share the same phase condition. Then, a slight index change in the external waveguide leads to a mode jump. In this particular example, we can switch from  $\lambda = 1.643$  to  $1.490 \mu\text{m}$  with only a few percentile variation in

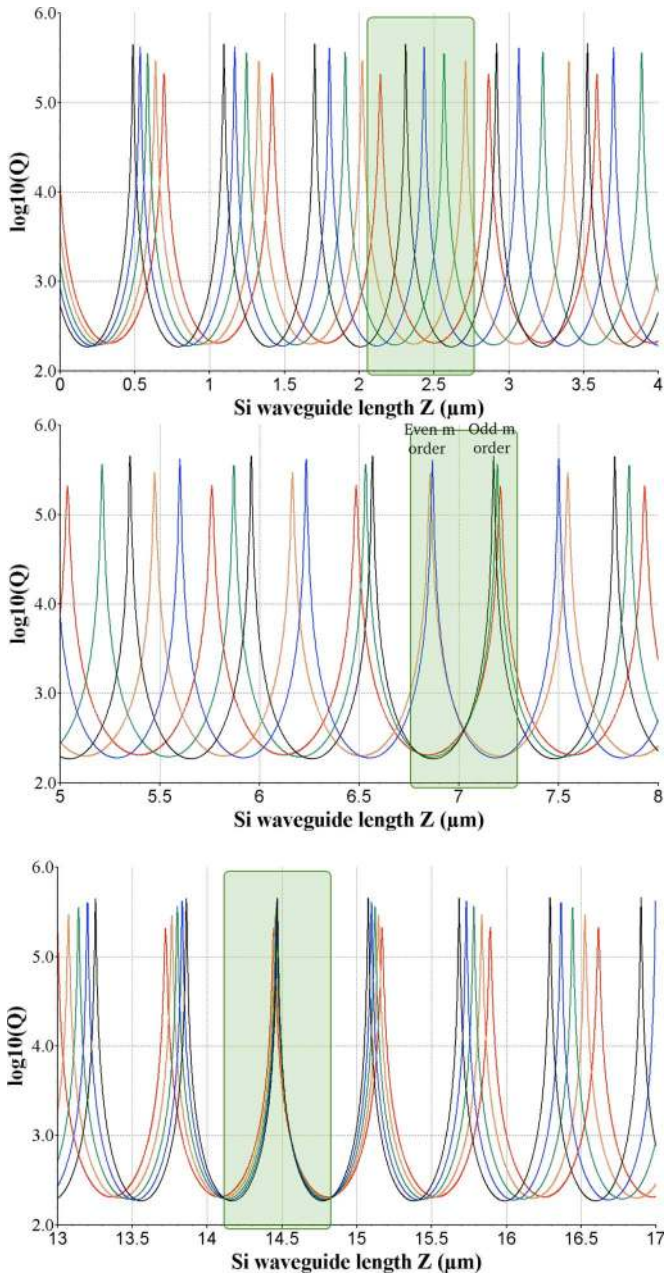


Fig. 9.  $Q$  factor variation as function of external loop length for resonant modes of a  $4\ \mu\text{m}$  radius and  $0.55\text{-}\mu\text{m}$ -thick microdisk coupled to a  $200 \times 500\ \text{nm}$  Si waveguide. Differently colored curves corresponds to the  $\text{TE}(0,31,0) = 1645\ \text{nm}$  up to the  $\text{TE}(0,35,0) = 1490\ \text{nm}$  resonances of the resonator. The minimum value of  $Q$  can be arbitrary low and is determined by the coupling rate.

the optical paths (i.e.,  $Z$  from  $14.44$  to  $14.47\ \mu\text{m}$  in terms of waveguide lengths). If the FSR of the microdisk corresponds to the channel spacing in the communication system, we can now hop to the different channels by using only a very small refractive index change.

### III. ADVANCED FUNCTIONALITY OF MDL

#### A. Microdisk Electrooptical Switch

Also low-power optical switching is an essential network functionality. Here, we demonstrate that a MDL coupled to two

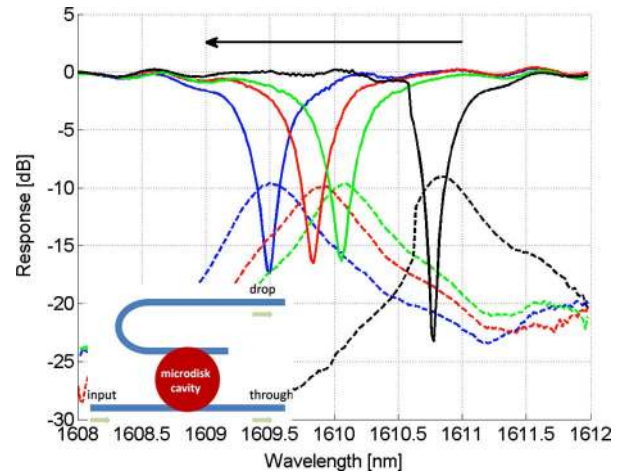


Fig. 10. Schematic layout of the proposed switch (inset) and the influence of the injection current on the through (solid) and drop (dashed) port transmission characteristics of the microdisk cavity [curves for  $0$ ,  $55\ \mu\text{A}$  ( $0.9\ \text{V}$ ),  $100\ \mu\text{A}$  ( $1\ \text{V}$ ), and  $200\ \mu\text{A}$  ( $1.1\ \text{V}$ )].

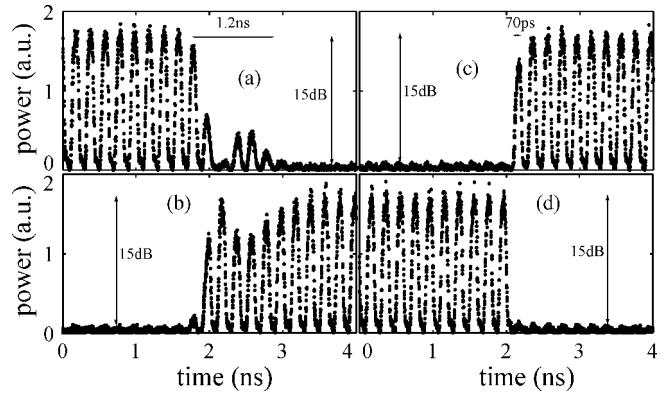


Fig. 11. Switching characteristics of the microdisk electrooptical switch. (a) and (c) are the off and on transients at the through port, respectively. (b) and (d) are the on and off transients at the drop port, respectively

bus waveguides [see Fig. 10(a)] can be used to switch an input digital signal between two outputs. The switching is based on the plasma dispersion effect, which induces a shift in the resonance wavelength when injecting current in the microdisk cavity. The experiments were carried out using a  $10\text{-}\mu\text{m}$  diameter microdisk. Forward biasing the microdisk blue shifts the resonance, as shown in Fig. 10. The best working point for switching was found to be  $55\ \mu\text{A}$  ( $0.9\ \text{V}$ ). The bandwidth of the switch at resonance was  $0.7\ \text{nm}$ , in principle allowing to switch  $10\ \text{Gb/s}$  and even  $40\ \text{Gb/s}$  data signals. In the current device, the drop port loss was  $10\ \text{dB}$ , which is probably due to a slight unbalance between the coupling coefficients to the bus waveguides related to a misalignment in the microdisk fabrication. To demonstrate the dynamic response of the proposed switch, we used a  $10\ \text{GHz}$  periodically modulated optical signal (center wavelength at  $1610.19\ \text{nm}$ ) as the input beam, and the bias of the microdisk was swept from  $-1.1\ \text{V}$  (negligible current) to  $+0.9\ \text{V}$  ( $55\ \mu\text{A}$ ). The results are shown in Fig. 11. Switching from drop port to through port takes about  $70\ \text{ps}$ . However, in the opposite direction the switching time is about  $1.2\ \text{ns}$  due to the relaxation oscillation

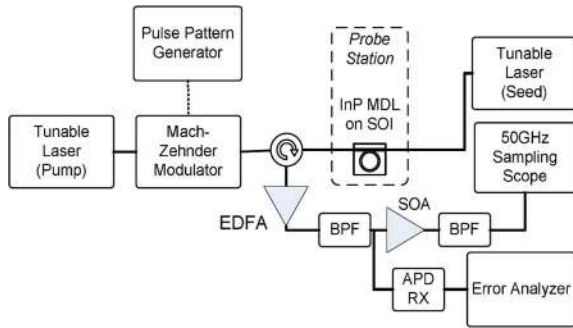


Fig. 12. Experimental setup for microdisk-based all-optical wavelength conversion (from [40]).

in the carrier-injection transient. The dynamic extinction ratio is about 15 dB, similar to that of the static case, as shown in Fig. 10.

### B. All-Optical Wavelength Conversion

To improve the scalability of wavelength-routed networks, all-optical wavelength conversion is an important function [15]. In [39], we demonstrated for the first time that the MDL can be used as an ultralow power wavelength converter. Static wavelength conversion with a control power of  $6.4 \mu\text{W}$  and dynamic conversion using a 5 Gb/s nonreturn-to-zero bit sequence was demonstrated. Recently, we improved these results further and demonstrated up to 10 Gb/s wavelength conversion [40] (using first generation MDLs). The experimental setup is shown in Fig. 12. The pump signal was tuned to a nondominant lasing mode of the MDL. The converted signal (at the dominant laser mode) is extracted using a circulator and is inverted with respect to the input signal. In this second experiment, we also added a seed laser (tuned to the dominant laser mode), which supports the recovery of the laser signal.

Using this setup, we measured the bit error rate at 2.5 Gb/s. Due to the weak output power, the bit error rate at 10 Gb/s could not be determined, but clearly inverted signals were obtained using a sampling scope.

### C. All-Optical Flip-Flops

It has been shown before that ring or disk lasers can be used to implement all-optical flip-flops (AOFFs) [41], with switching taking place between two unidirectional (clockwise and counterclockwise) lasing states. Theoretical work has revealed however that such unidirectional operation is only possible if the coupling between the clockwise and the counterclockwise lasing modes is sufficiently small and if the photon density in the lasing mode is sufficiently large [42].

In the heterogeneously integrated MDLs described earlier, we can obtain high power density in the whispering gallery mode owing to the high index contrast of the InP membranes. Due to the improved heat sinking obtained through the thick top contact, we can also drive the MDLs up to relatively high currents and high power levels.

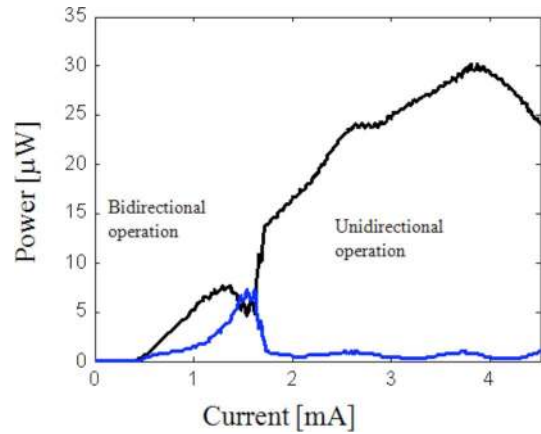


Fig. 13. Typical output power versus current characteristic of a MDL for AOFF operation, measured at both ends of the SOI waveguide.

Coupling between clockwise and counterclockwise modes is mainly caused by the scattering at the disk surface and by the reflections in the silicon waveguides at the grating couplers. This coupling was substantially reduced when using the optimized lithography and etching processes discussed in Section II, resulting in minimum sidewall surface roughness. In addition, we have employed a relatively thick (250 nm) divinylsiloxane (DVS)-BCB bonding layer to reduce the coupling between disk and straight SOI waveguides, and thus, to reduce the influence of the reflections at the grating couplers.

A typical power versus current characteristic, measured at both ends of the silicon waveguide, is shown in Fig. 13. Unidirectional operation is obtained from 1.7 mA onward. Due to the single-mode operation of the laser, we did not observe any switching of the unidirectional operation when changing the bias current.

Switching between clockwise and counterclockwise modes in disk and ring lasers is achieved through injection locking. Optical pulses at the laser wavelength injected at the left, respectively, right-hand side lock the counterclockwise, respectively, clockwise laser mode and cause switching off of the clockwise, respectively, counterclockwise mode. We performed switching experiments using 100 ps long set and reset pulses, which were alternatively injected to the left and the right grating couplers and biased the MDL at 3.5 mA (roughly twice the threshold for unidirectional operation). The output power measured from the right grating coupler, showing switching on and off of the clockwise mode, is shown in Fig. 14. Due to the design of the device (with only one straight waveguide coupled to the disk), it was not possible to separate the switching pulses and the laser output. Switching was obtained in less than 100 ps using pulses with an energy of only 1.8 fJ. For more details, we refer to [43].

### D. Optical Gating

Optical gating can be implemented using the MDLs below their lasing threshold current or even without or with negative bias. In both cases, it is based on carrier density changes induced by the data, which cause changes in the microdisk resonances that are in turn affecting the transmission of clock pulses.

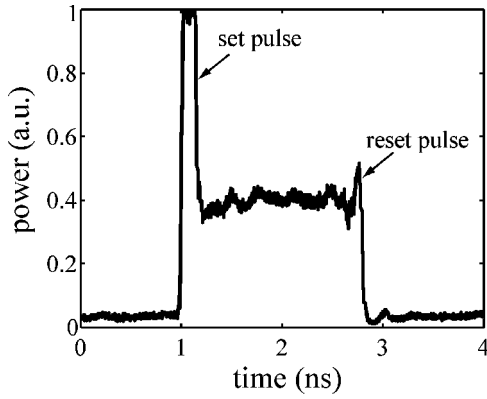


Fig. 14. Switching on and off of the MDL, at a bias current of 3.5 mA and using 100 ps long pulses.

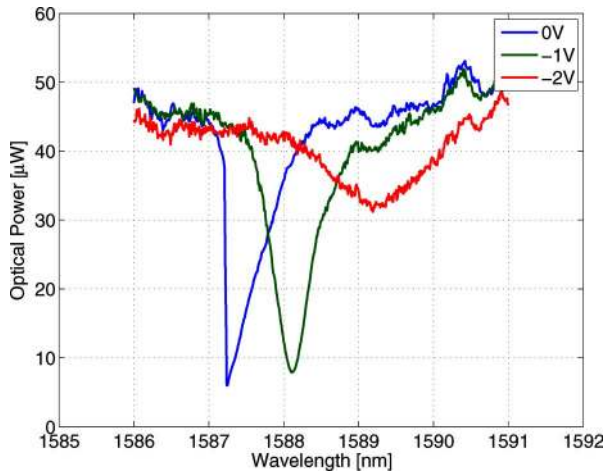


Fig. 15. Transmission at the through port of a negatively or zero-biased MDL versus wavelength of the probe beam.

We performed gating experiments using MDLs with 10  $\mu\text{m}$  radius and the improved design described in Section II-B. We applied a bias varying from 0 to  $-2$  V and used a CW probe beam in combination with a pump beam consisting of 10 GHz pulses. Fig. 15 shows the transmission at the through port versus wavelength for bias voltages of  $-2$ ,  $-1$ , and 0 V and for a probe beam of 0.5 mW, which fully saturates the absorption. Rise and fall times together were 50 ps.

#### IV. PASSIVE OPTICAL ROUTING DEVICES

##### A. Fabrication Accuracy of Silicon Nanophotonic Circuits

One of the major drawbacks of high index contrast waveguide platforms is the very limited tolerance for manufacturing imperfections. Slight deviations in device dimensions (height and width) can cause considerable shift in the spectral response of the filters used for routing and selecting wavelength channels. In complex circuits, such as those proposed for on-chip optical networks [11]–[13], which consists of a concatenation of multiple wavelength dependent devices, this leads to high losses or even errors in the routing process. We investigated in detail the performance of the currently available process, based

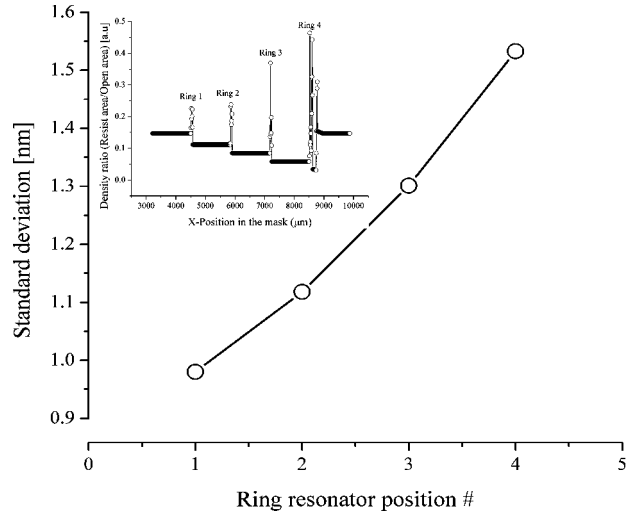


Fig. 16. Nonuniformity of four ring resonators with different local pattern density over a 200 mm wafer. The inset shows the local pattern density.

on 193 nm DUV lithography and dry etching [30]. We found that the variations manifest themselves at two different levels: variations over a single die and variations over a wafer. At both levels, the photolithography and the dry etching process are the two main causes for linewidth variations during pattern definition. Next to these, waveguide thickness variations originating from the base wafer (SOI) may further induce resonant wavelength variations. By careful process design, the nonuniformity of the devices can be improved considerably. We have demonstrated that a device nonuniformity of  $<0.6$  nm within a die and  $<2$  nm within a wafer can be achieved [44], [45]. However, further enhancement requires improvement of the circuit design. To illustrate this, we investigated a design containing four ring resonators separated by 1.5 mm. In the neighborhood of the ring resonators, the overall device density (density of patterns around the ring resonators under study) changes abruptly. The design was set up in such a way that this change was relatively small in the neighborhood of the first ring, and then, gradually increased toward the fourth ring. We then measured the uniformity of the resonance wavelength of the four rings from 11 chips selected from a single 200 mm wafer.

To avoid any environmental disturbances, the circuits were characterized in a clean-room environment. From the results in Fig. 16, it can be clearly seen that abrupt changes in the device density (ring 4) create considerable device nonuniformity ( $\sigma = 1.55$  nm), while ring 1, which had the lowest variation has also lower nonuniformity ( $\sigma = 0.98$  nm). Thus, designing the circuits in such a way that the device density is kept as uniform as possible is important in achieving the optimum uniformity.

As a further test for the high-resolution fabrication process, we designed higher order ring resonator-based filters. Both coupled cavity filters (CCF) and all-pass filters (APF) were implemented, using race-track resonators as the base element. In case of the CCF, from 10 up to 30 identical ring resonators were side coupled to each other and the coupling gap between the resonators was tuned to reduce the passband ripple [46]. Fig. 17 depicts the spectral response of a tenth order CCF filter. Despite



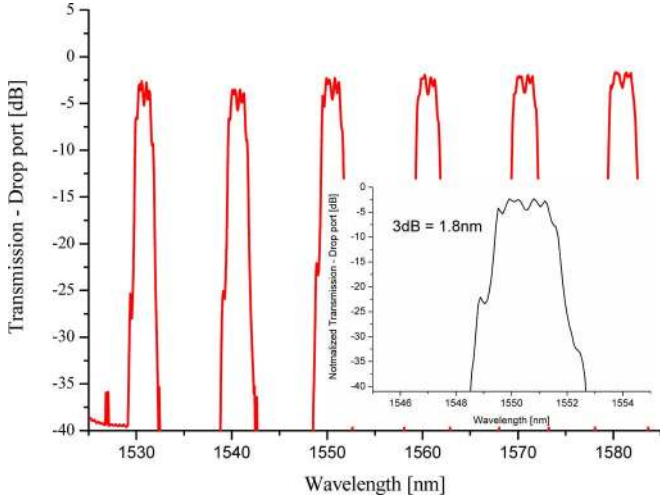


Fig. 17. Spectral response of a tenth order CCF, inset shows details of a single wavelength band.

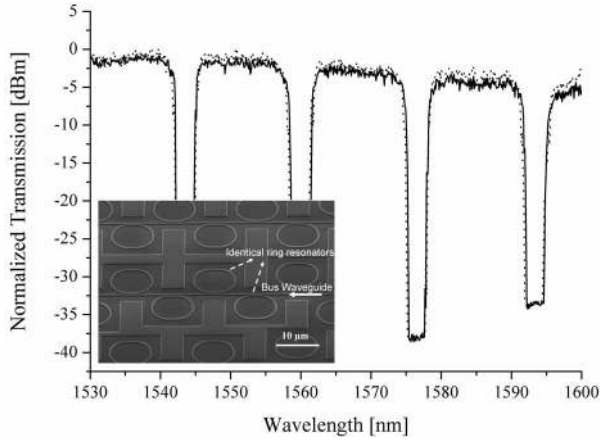


Fig. 18. Spectral response of two APF devices with 200 identical race-track ring resonators coupled to a common bus waveguide. Inset shows SEM picture of the APF.

the variation in the coupling rate, a passband ripple of approximately 2 dB is observed, which we believe to be related to mask discretization errors (a 5 nm grid was used). The increased passband width of these filters [1.8 nm full-width at half-maximum (FWHM)] can be used to compensate for variations in the laser wavelengths or filter resonances. The APF configuration is implemented by cascading identical race-track ring resonators to a common bus waveguide (see inset Fig. 18). The spectral response of two identical APFs with 200 rings each is shown in Fig. 18. The response of the two filters is very similar, which demonstrates the uniformity of the fabrication process.

In literature, it was suggested that these devices can be used as a compact optical buffer [47]. Therefore, we also measured the optical delay through higher order APFs and CCFs with up to 200 resonators for which we found a delay of 6.0 and 1.2 ps/ring, respectively. Even though the APF configuration yields substantial higher delays, the insertion loss at resonance is very high making them at this moment impractical for implementing an optical buffer.

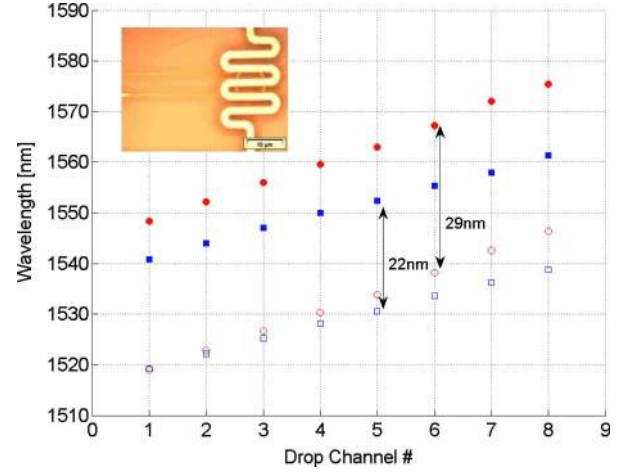


Fig. 19. Experimentally measured channel wavelengths for two 8-channel add-drop multiplexers with 29 nm (circles) and 22 nm (squares) FSR, respectively. The inset shows a microscope image of the fabricated heater with underlying ring resonator.

### B. Thermal Tuning of Silicon Nanophotonic Circuit

Despite the progress in fabrication technology, in many cases further fine-tuning of the wavelength selective devices is required. Here, we present thermo-optic tuning of microring-based filters. The filters and the heaters discussed in this section, were fabricated using 248 nm DUV lithography. Following definition of the waveguides, they were covered by SiO<sub>2</sub> grown at low temperature and further planarized by chemical mechanical polishing. A 550-nm-thick layer remained on top of the microring resonators, which is a compromise between minimizing the optical loss and optimizing the heat transfer. The heaters consist of a 100-nm-thick titanium layer (sheet resistance of 6 Ω/□), which is compatible with the fabrication constraints of the CMOS pilot line. The inset of Fig. 19 shows a top view of the fabricated device.

Taking into account a thermo-optic effect  $dn/dT = +1.8 \times 10^{-4} \text{ K}^{-1}$  for silicon, we expect a spectral shift of 0.1 nm/°C for the silicon ring resonators. We simulated the proposed heater using a finite-element method and found a thermal resistance of 4600 °C/W for the 2 μm silica layer between the titanium heater and the silicon substrate in which the silicon waveguide is encapsulated. We also derived that 10 mW heat dissipation leads to an increase of the heater temperature by 46 °C. The temperature of the silicon ring resonator, which is 550 nm below, increases by up to 35 °C. Therefore, the theoretically expected spectral shift is 0.35 nm/mW.

The ring resonators of the eight-channel add-drop were designed to have either a FSR of 32 nm or 23 nm. Within the same circuit, slight changes in the microring radii ensure a channel spacing  $\Delta\lambda$  between adjacent channels of 4 nm (FSR = 32 nm) or 3 nm (FSR = 23 nm) to cover the whole FSR. Fig. 19 shows the experimentally measured FSR (29 and 22 nm, respectively) and channel spacing (3.3 and 2.8 nm, respectively). The slight deviation between simulated and measured values is related to an underestimation of the waveguide group index.

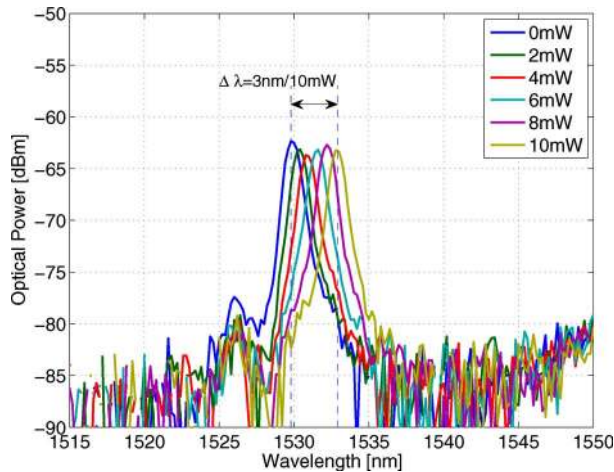


Fig. 20. Tuning of spectral response for increasing power consumption.

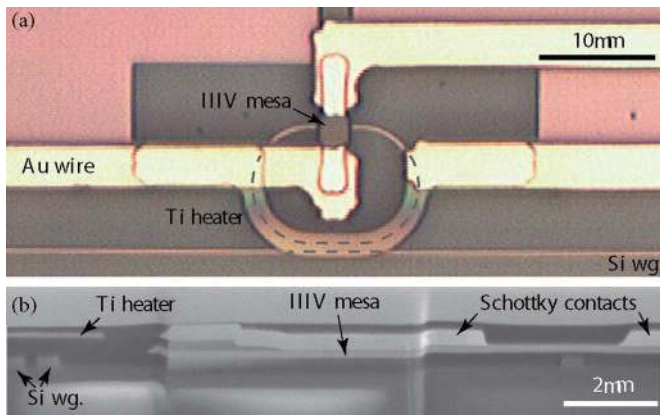
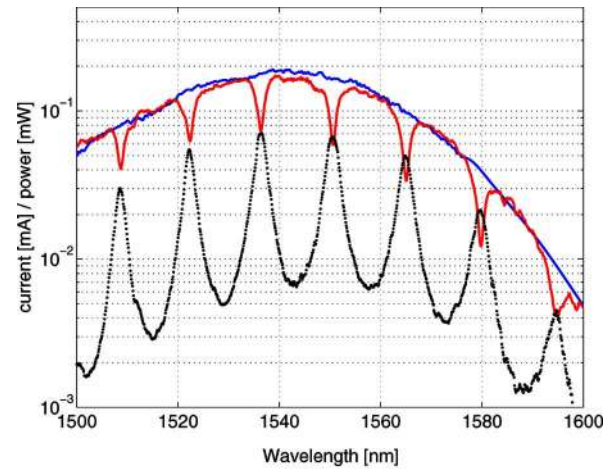


Fig. 21. (a) Top view and (b) cross-sectional view of a fully fabricated resonant detector.

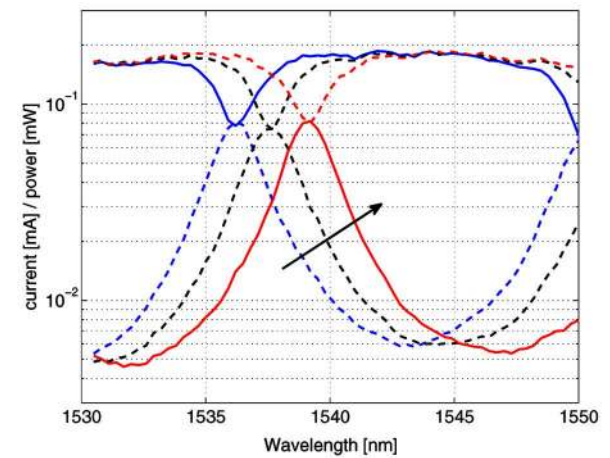
Tuning of the microring resonant wavelength by dissipating power in the heater is shown in Fig. 20. A linear red shift of 0.3 nm/mW is observed, which correspond to an efficiency of 26  $\mu\text{W}/\text{GHz}$ , comparable with the best values reported in literature [48] and [49]. The maximum power that can be dissipated in the heaters is 40 mW, so tuning over the full channel spacing is possible without any problem. We confirmed that there is no thermal crosstalk between two adjacent ring resonators, which were spaced 200  $\mu\text{m}$  apart (center-to-center).

## V. WAVELENGTH SELECTIVE DETECTORS

Wavelength selective detection is necessary for the aforementioned optical interconnect involving WDM and wavelength routing networks. We recently demonstrated a compact resonant metal-semiconductor-metal photodetector by integrating a short III-V absorbing mesa directly onto an SOI ring resonator [50]. Here, we further expand the functionality of this device by integrating a local heater for tuning the detection wavelength. Fig. 21 shows some pictures of a fabricated device. The InGaAs absorption layer was first bonded on top of the SOI circuits by using DVS-BCB polymer (see [51] for details on layer structure). Then the mesa, with a width of 3  $\mu\text{m}$ , was



(a)



(b)

Fig. 22. (a) Measured transmission spectrum and detected current of a fabricated device. Solid line indicates the incident power spectrum, dashed lines indicate the transmission spectrum, and dotted lines indicate the detected current. Since grating couplers were used to interface to the access fibers, the input light follows a Gaussian spectrum (b) Transmission and current at different electrical powers applied to the heater. Along the arrow direction, the applied powers are 0, 4.2, and 8.2 mW, respectively.

defined by optical lithography and wet chemical etching. In the next step, a DVS-BCB overladding layer was spun onto the whole chip for isolating the SOI circuits from the metal wires. A via was opened on top of the III-V mesa. A 100-nm-thick Ti layer (heater) was subsequently deposited on some part of the SOI ring. Finally, a Ti/Au metal layer was deposited to form the Schottky contacts and the wiring.

Fig. 22(a) shows the optical transmission and the detected current of a fabricated device at a bias voltage of 7 V. Obviously, the detected current shows a wavelength selective response. At the resonant wavelength, the detector responsivity reaches 0.47 mA/mW. Off resonance, the detected current drops by about 10 dB. In the transmission spectrum, resonant dips can also be observed, but the extinction ratio is only about 6–10 dB. Note that the responsivity and extinction ratio shown here do not yet reach the theoretical optimum. By carefully designing the coupling ratios from the ring cavity to the SOI bus waveguide

and to the III–V absorption mesa, up to 1 A/W has been achieved [50]. The present device also exhibits a shoulder voltage of 3 V, and a dark current of 0.1 nA up to 10 V bias. By sending a current through the integrated Ti heater, the resonant wavelength of the present device can be tuned, as shown in Fig. 22(b). A maximum red shift of 3 nm was obtained by applying an electrical power of 8.2 mW to the heater. No degradation of the responsivity or dark current was observed up to this point. Although the amount of tuning is still not sufficient to cover the whole FSR of the ring cavity, it can be used as a trimming method to compensate the wavelength drift from, e.g., fabrication errors.

## VI. CONCLUSION

We described the design and operation of a MDL, fabricated using heterogeneous operation and its possible application in compact optical networks. Through improved design and processing, the threshold current could be decreased to 350  $\mu$ A and the output power under CW operation increased to 120  $\mu$ W. The latter in turn allowed to demonstrate more advanced functionality, needed for scaling up the optical network capacity, such as all-optical wavelength conversion at high speed and optical flip-flop operation. Next, we discussed the passive waveguide circuit fabrication process, its robustness versus fabrication variations and the implementation of thermal tuning to overcome these variations. Finally, we proposed a tunable resonant detector, which may become an essential component in wavelength-routed networks.

## REFERENCES

- [1] F. E. Doany, C. L. Schow, C. W. Baks, D. A. Kuchta, P. Pepeljugoski, L. Schares, R. Budd, F. Libsch, R. Dangel, F. Horst, B. J. Offrein, and J. A. Kash, "160 Gb/s bidirectional polymer-waveguide board-level optical interconnects using CMOS-based transceivers," *IEEE Trans. Adv. Packag.*, vol. 32, no. 2, pp. 345–359, May 2009.
- [2] A. Suzuki, Y. Wakazono, T. Ishikawa, Y. Hashimoto, H. Masuda, S. Suzuki, M. Tamura, T. Suzuki, K. Kikuchi, H. Nakagawa, M. Aoyagi, and T. Mikawa, "Low-cost optical subassembly using VCSEL pre-self-aligned with optical fiber for optical interconnect applications," *J. Lightw. Technol.*, vol. 27, no. 20, pp. 4516–4523, Oct. 2009.
- [3] Y. A. Vlasov and S. J. McNab, "Losses in single-mode silicon-on-insulator strip waveguides and bends," *Opt. Exp.*, vol. 12, pp. 1622–1631, Apr. 2004.
- [4] W. Bogaerts, S. K. Selvaraja, P. Dumon, J. Brouckaert, K. De Vos, D. Van Thourhout, and R. Baets, "Silicon-on-insulator spectral filters fabricated with CMOS technology," *J. Sel. Top. Quantum Electron.*, vol. 16, no. 1, pp. 33–44, Jan./Feb. 2010.
- [5] T. Tsuchizawa, K. Yamada, H. Fukuda, T. Watanabe, T. Jun-Ichi, M. Takahashi, T. Shoji, E. Tamechika, S. Itabashi, and H. Morita, "Microphotonics devices based on silicon microfabrication technology," *IEEE J. Sel. Topics Quantum Electron.*, vol. 11, no. 1, pp. 232–240, Jan./Feb. 2005.
- [6] M. Lipson, "Compact electro-optic modulators on a silicon chip," *IEEE J. Sel. Topics Quantum Electron.*, vol. 12, no. 6, pp. 1520–1526, Nov./Dec. 2006.
- [7] W. M. J. Green, M. J. Rooks, L. Sekaric, and Y. A. Vlasov, "Ultra-compact, low RF power, 10 Gb/s silicon mach-zehnder modulator," *Opt. Exp.*, vol. 15, pp. 17106–17113, Dec. 2007.
- [8] D. Marris-Morini, L. Vivien, G. Rasigade, J. M. Fedeli, E. Cassan, X. Le Roux, P. Crozat, S. Maine, A. Lupu, P. Lyan, P. Rivallin, M. Halbwax, and S. Laval, "Recent progress in high-speed silicon-based optical modulators," *Proc. IEEE*, vol. 97, no. 7, pp. 1199–1215, Jul. 2009.
- [9] L. Vivien, J. Osmond, J. M. Fedeli, D. Marris-Morini, P. Crozat, J. F. Damlencourt, E. Cassan, Y. Lecunff, and S. Laval, "42 GHz p.i.n Germanium photodetector integrated in a silicon-on-insulator waveguide," *Opt. Exp.*, vol. 17, pp. 6252–6257, Apr. 2009.
- [10] L. Chen, K. Preston, S. Manipatruni, and M. Lipson, "Integrated GHz silicon photonic interconnect with micrometer-scale modulators and detectors," *Opt. Exp.*, vol. 17, pp. 15248–15256, Aug. 2009.
- [11] O. Liboiron-Ladouceur, H. Wang, A. S. Garg, and K. Bergman, "Low-power, transparent optical network interface for high bandwidth off-chip interconnects," *Opt. Exp.*, vol. 17, pp. 6550–6561, Apr. 2009.
- [12] A. V. Krishnamoorthy, R. Ho, X. Z. Zheng, H. Schwetman, J. Lexau, P. Koka, G. L. Li, I. Shubin, and J. E. Cunningham, "Computer systems based on silicon photonic interconnects," *Proc. IEEE*, vol. 97, no. 7, pp. 1337–1361, Jul. 2009.
- [13] J. Ahn, M. Fiorentino, R. G. Beausoleil, N. Binkert, A. Davis, D. Fattal, N. P. Jouppi, M. McLaren, C. M. Santori, R. S. Schreiber, S. M. Spillane, D. Vantrease, and Q. Xu, "Devices and architectures for photonic chip-scale integration," *Appl. Phys. A-Mater. Sci. Process.*, vol. 95, pp. 989–997, Jun. 2009.
- [14] D. A. B. Miller, "Device requirements for optical interconnects to silicon chips," *Proc. IEEE*, vol. 97, no. 7, pp. 1166–1185, Jul. 2009.
- [15] W. D. Zhong and R. S. Tucker, "Wavelength routing-based photonic packet buffers and their applications in photonic packet switching systems," *J. Lightw. Technol.*, vol. 16, no. 10, pp. 1737–1745, 1998.
- [16] T. Mitze, M. Schnarrenberger, L. Zimmermann, J. Bruns, F. Fidorra, K. Janiak, J. Kreissl, S. Fidorra, H. Heidrich, and K. Petermann, "CWDM transmitter module based on hybrid integration," *IEEE J. Sel. Topics Quantum Electron.*, vol. 12, no. 5, pp. 983–987, Sep./Oct. 2006.
- [17] C. G. Fonstad, J. J. Rimpler, E. R. Barkley, J. M. Perkins, and S. Famenini, "Recess integration of micro-cleaved laser diode platelets with dielectric waveguides on silicon – art. no. 69090 O," in *Proc. Conf. Novel in-Plane Semicond. Lasers VII*, San Jose, CA, 2008, pp. O9090–O9090.
- [18] N. Jockerst, M. Royal, S. Palit, L. Luan, S. Dhar, and T. Tyler, "Chip scale integrated microresonator sensing systems," *J. Biophoton.*, vol. 2, pp. 212–226, Apr. 2009.
- [19] G. Roelkens, J. Brouckaert, D. Taillaert, P. Dumon, W. Bogaerts, D. Van Thourhout, R. Baets, R. Notzel, and M. Smit, "Integration of InP/InGaAsP photodetectors onto silicon-on-insulator waveguide circuits," *Opt. Exp.*, vol. 13, pp. 10102–10108, Dec. 12, 2005.
- [20] A. W. Fang, M. N. Sysak, B. R. Koch, R. Jones, E. Lively, Y. H. Kuo, D. Liang, O. Raday, and J. E. Bowers, "Single-wavelength silicon evanescent lasers," *IEEE J. Sel. Topics Quantum Electron.*, vol. 15, no. 3, pp. 535–544, May/June 2009.
- [21] T. Okumura, T. Maruyama, M. Kanemaru, S. Sakamoto, and S. Arai, "Single-mode operation of GaInAsP/InP-membrane distributed feedback lasers bonded on silicon-on-insulator substrate with rib-waveguide structure," *Jpn. J. Appl. Phys. Part 2-Lett. Exp. Lett.*, vol. 46, pp. L1206–L1208, Dec. 2007.
- [22] D. Liang, J. E. Bowers, D. C. Oakley, A. Napoleone, D. C. Chapman, C. L. Chen, P. W. Juodawlkis, and O. Raday, "High-quality 150 nm InP-to-silicon epitaxial transfer for silicon photonic integrated circuits," *Electrochem. Solid State Lett.*, vol. 12, pp. H101–H104, 2009.
- [23] M. Kostrzewa, L. Di Cioccio, M. Zussy, J. C. Roussin, J. M. Fedeli, N. Kernevez, P. Regreny, C. Lagahe-Blanchard, and B. Aspar, "InP dies transferred onto silicon substrate for optical interconnects application," *Sens. Actuators A-Phys.*, vol. 125, pp. 411–414, Jan. 2006.
- [24] G. Roelkens, J. Brouckaert, D. Van Thourhout, R. Baets, R. Notzel, and M. Smit, "Adhesive bonding of InP/InGaAsP dies to processed silicon-on-insulator wafers using DVS-bis-benzocyclobutene," *J. Electrochem. Soc.*, vol. 153, pp. G1015–G1019, 2006.
- [25] S. L. McCall, A. F. J. Levi, R. E. Slusher, S. J. Pearton, and R. A. Logan, "Whispering gallery mode microdisk lasers," *Appl. Phys. Lett.*, vol. 60, pp. 289–291, 1992.
- [26] C. Seassal, P. Rojo-Romeo, X. Letartre, P. Viktorovitch, G. Hollinger, E. Jalaguier, S. Pocas, and B. Aspar, "InP microdisk lasers on silicon wafer: CW room temperature operation at 1.6  $\mu$ m," *Electron. Lett.*, vol. 37, pp. 222–223, Feb. 2001.
- [27] H. T. Hattori, C. Seassal, E. Touraille, P. Rojo-Romeo, X. Letartre, G. Hollinger, P. Viktorovitch, L. Di Cioccio, M. Zussy, L. El Melhaoui, and J. M. Fedeli, "Heterogeneous integration of microdisk lasers on silicon strip waveguides for optical interconnects," *IEEE Photon. Technol. Lett.*, vol. 18, no. 1, pp. 223–225, Jan./Feb. 2006.
- [28] P. R. Romeo, J. Van Campenhout, P. Regreny, A. Kazmierczak, C. Seassal, X. Letartre, G. Hollinger, D. Van Thourhout, R. Baets, M. Fedeli, and L. Di Cioccio, "Heterogeneous integration of electrically driven microdisk based laser sources for optical interconnects and photonic ICs," *Opt. Exp.*, vol. 14, pp. 3864–3871, May 2006.
- [29] J. Van Campenhout, P. Rojo-Romeo, P. Regreny, C. Seassal, D. Van Thourhout, S. Verstyft, L. Di Cioccio, J. M. Fedeli, C. Lagahe, and

- R. Baets, "Electrically pumped InP-based microdisk lasers integrated with a nanophotonic silicon-on-insulator waveguide circuit," *Opt. Exp.*, vol. 15, pp. 6744–6749, May 2007.
- [30] S. K. Selvaraja, P. Jaenen, W. Bogaerts, D. Van Thourhout, P. Dumon, and R. Baets, "Fabrication of photonic wire and crystal circuits in silicon-on-insulator using 193-nm optical lithography," *J. Lightw. Technol.*, vol. 27, no. 18, pp. 4076–4083, Sep. 2009.
- [31] F. Mandorlo, P. Rojo-Romeo, X. Letarte, and P. Viktorovitch, "A simple perturbative analysis for fast design of an electrically pumped microdisk laser," *Opt. Exp.*, vol. 17, pp. 70–79, Jan. 2009.
- [32] J. E. Heebner, T. C. Bond, and J. S. Kallman, "Generalized formulation for performance degradations due to bending and edge scattering loss in microdisk resonators," *Opt. Exp.*, vol. 15, pp. 4452–4473, Apr. 2007.
- [33] J. Van Campenhout, P. Rojo-Romeo, D. Van Thourhout, C. Seassal, P. Regreny, L. Di Cioccio, J. M. Fedeli, and R. Baets, "Thermal characterization of electrically injected thin-film InGaAsP microdisk lasers on Si," *J. Lightw. Technol.*, vol. 25, no. 6, pp. 1543–1548, Jun. 2007.
- [34] D. Taillaert, F. Van Laere, M. Ayre, W. Bogaerts, D. Van Thourhout, P. Bienstman, and R. Baets, "Grating couplers for coupling between optical fibers and nanophotonic waveguides," *Jpn. J. Appl. Phys. Part 1-Reg. Papers Brief Commun. Rev. Papers*, vol. 45, pp. 6071–6077, Aug. 2006.
- [35] J. Van Campenhout, L. Liu, P. R. Romeo, D. Van Thourhout, C. Seassal, P. Regreny, L. Di Cioccio, J. M. Fedeli, and R. Baets, "A compact SOI-integrated multiwavelength laser source based on cascaded InP microdisks," *IEEE Photon. Technol. Lett.*, vol. 20, no. 16, pp. 1345–1347, Jul./Aug. 2008.
- [36] L. Liu, G. Roelkens, J. Van Campenhout, J. Brouckaert, D. Van Thourhout, and R. Baets, "III–V/silicon-on-insulator nanophotonic cavities for optical network-on-chip," *J. Nanosci. Nanotechnol.*, vol. 10, pp. 1461–1472, 2010.
- [37] F. Mandorlo, P. Rojo-Romeo, X. Letarte, J. M. Fedeli, and P. Viktorovitch, "Improvement of threshold and mode selectivity of a microdisk laser by engineering its coupling to an external passive cavity," presented at the Group IV Photon., San Francisco, CA, 2009.
- [38] C. Manolatu, M. J. Khan, S. H. Fan, P. R. Villeneuve, H. A. Haus, and J. D. Joannopoulos, "Coupling of modes analysis of resonant channel add-drop filters," *IEEE J. Quantum Electron.*, vol. 35, no. 9, pp. 1322–1331, Sep. 1999.
- [39] L. Liu, J. Van Campenhout, G. Roelkens, D. Van Thourhout, P. Rojo-Romeo, P. Regreny, C. Seassal, J. M. Fedeli, and R. Baets, "Ultralow-power all-optical wavelength conversion in a silicon-on-insulator waveguide based on a heterogeneously integrated III–V microdisk laser," *Appl. Phys. Lett.*, vol. 93, article no. 061107, Aug. 2008.
- [40] O. Raz, L. Liu, D. Van Thourhout, P. Rojo-Romeo, J. M. Fedeli, and H. J. S. Dorren, "High speed wavelength conversion in a heterogeneously integrated disc laser over silicon on insulator for network on a chip applications," in *Proc. Eur. Conf. Opt. Commun.*, Vienna, Austria, 2009, p. 4.2.3.
- [41] M. Sorel, P. J. R. Laybourn, G. Giuliani, and S. Donati, "Unidirectional bistability in semiconductor waveguide ring lasers," *Appl. Phys. Lett.*, vol. 80, pp. 3051–3053, Apr. 2002.
- [42] M. Sorel, G. Giuliani, A. Scire, R. Miglierina, S. Donati, and P. J. R. Laybourn, "Operating regimes of GaAs–AlGaAs semiconductor ring lasers: Experiment and model," *IEEE J. Quantum Electron.*, vol. 39, no. 10, pp. 1187–1195, Oct. 2003.
- [43] L. Liu, R. Kumar, K. Huybrechts, T. Spuesens, G. Roelkens, E.-J. Geluk, T. de Vries, P. Regreny, D. Van Thourhout, R. Baets, and G. Morthier, "An ultra-small low power all-optical flip-flop memory on a silicon chip," *Nature Photon.* [Online]. Available: <http://dx.doi.org/10.1038/nphoton.2009.268>
- [44] S. K. Selvaraja, P. Jaenen, S. Beckx, W. Bogaert, P. Dumon, D. Van Thourhout, and R. Baets, "Silicon nanophotonic wire structures fabricated by 193 nm optical lithography," in *Proc. 20th Annu. Meet. IEEE Lasers Electro-Opt. Soc. (LEOS 2007)*, pp. 48–49.
- [45] S. K. Selvaraja, W. Bogaerts, P. Dumon, D. Van Thourhout, and R. G. Baets, "Subnanometer linewidth uniformity in silicon nanophotonic waveguide devices using CMOS fabrication technology," *J. Sel. Topics Quantum Electron.* DOI: 10.1109/JSTQE.2009.2026550.
- [46] F. N. Xia, M. Rooks, L. Sekaric, and Y. Vlasov, "Ultra-compact high order ring resonator filters using submicron silicon photonic wires for on-chip optical interconnects," *Opt. Exp.*, vol. 15, pp. 11934–11941, Sep. 17, 2007.
- [47] F. N. Xia, L. Sekaric, and Y. Vlasov, "Ultracompact optical buffers on a silicon chip," *Nature Photon.*, vol. 1, pp. 65–71, Jan. 2007.
- [48] F. Gan, T. Barwicz, M. A. Popovic, M. S. Dahlem, C. W. Holzwarth, P. T. Rakich, H. I. Smith, E. P. Ippen, F. X. Kartner, and I. Lee, "Maximizing the thermo-optic tuning range of silicon photonic structures," in *Proc. Photon. Switching 2007 Conf.*, San Francisco, CA, pp. 67–68.
- [49] I. Christiaens, D. Van Thourhout, and R. Baets, "Low-power thermo-optic tuning of vertically coupled microring resonators," *Electron. Lett.*, vol. 40, pp. 560–561, Apr. 2004.
- [50] L. Liu, J. Brouckaert, G. Roelkens, D. Van Thourhout, and R. Baets, "Compact, wavelength-selective resonant photodetector based on III–V/Silicon-on-insulator heterogeneous integration," presented at the Conf. Lasers Electro-Opt./Int. Quantum Electron. Conf. (CLEO), Baltimore, MD, 2009, paper CTuV3.
- [51] J. Brouckaert, G. Roelkens, D. Van Thourhout, and R. Baets, "Thin-film III–V photodetectors integrated on silicon-on-insulator photonic ICs," *J. Lightw. Technol.*, vol. 25, no. 4, pp. 1053–1060, Apr. 2007.

**Dries Van Thourhout** (M'98) received the Master's degree in physical engineering and the Ph.D. degree from Ghent University, Ghent, Belgium, in 1995 and 2000, respectively.

From October 2000 to September 2002, he was with Lucent Technologies, Bell Laboratories, Crawford Hill, NJ, where he was engaged in InPInGaAsP monolithically integrated devices. In October 2002, he joined the Department of Information Technology, Ghent University, where he is involved in integrated optoelectronic devices. His current research interests include heterogeneous integration by wafer bonding, intrachip optical interconnect, and wavelength-division multiplexing devices.

**Thijs Spuesens** (S'08–M'08) was born in Sas van Gent, The Netherlands, in 1982. He received the M.Sc. degree in electrical engineering from Eindhoven University of Technology, Eindhoven, The Netherlands, in 2008. He is currently working toward the Ph.D. degree in photonics in the Department of Information Technology (INTEC), Ghent University, Ghent, Belgium.

In August 2008, he joined the Photonics Research Group, INTEC. He is also involved in the FP7 project WADIMOS. His current research interests include heterogeneous integration of silicon-on-insulator and III–V material, optical interconnects, and microsources.

**Shankar Kumar Selvaraja** (S'06) received the M.Tech. degree in optical communication from the College of Engineering, Anna University, Chennai, India, in 2004, and the M.Sc. degree in microsystems and microelectronics from the University of Twente, Enschede, The Netherlands, in 2005. Since 2006, he is working toward the Ph.D. degree at Photonic Research Group, Interuniversity Microelectronics Center, Ghent University, Ghent, Belgium.

His current research interests include CMOS compatible process development for photonic integrated circuits: optical lithography (193 and 248 nm), dry etch, and deposition process.

Mr. Selvaraja is a Student Member of IEEE Photonics Society.



**Liu Liu** received the B.Eng. degree in information engineering from Zhejiang University, Hangzhou, China, in 2002, and the Ph.D. degree in photonics from Royal Institute of Technology, Stockholm, Sweden, in 2006.

From 2007 to 2009, he was a Postdoctoral Researcher with Photonics Research Group, Department of Information Technology, Ghent University, Ghent, Belgium. He is currently in the Department of Photonics Engineering, Technical University of Denmark, Lyngby, Denmark. His research interests

include heterogeneous integration and silicon nanophotonic devices.



**Günther Roelkens** (S'02–M'07) was born in Ghent, Belgium, in 1979. He received the M.Sc. degree in electrical engineering in 2002 and the Ph.D. degree in electrical engineering in April 2007, both from Ghent University, Ghent, Belgium

Since 2002, he has been with Photonics Research Group, Ghent University. He is also an Assistant Professor at the Technical University Eindhoven, Eindhoven, The Netherlands.

Dr. Roelkens was recipient of the Barco/Research Foundation Flanders (FWO) Award.

**Rajesh Kumar** received the B.Sc. and B.Ed. degrees in physical science from the Regional Institute of Education, Ajmer, India, in 2004, the M.Sc. degree in physics, and the M.Tech. degree in optoelectronics and optical communication from Indian Institute of Technology Delhi, New Delhi, India, in 2006 and 2008, respectively.

He was engaged in metal-oxide semiconductor thin films. He is currently in the Department of Information Technology, Interuniversity Microelectronics Center, Ghent University, Ghent, Belgium. His current research interests include microdisk-based photonic components and devices for optical communication.

Mr. Kumar is Student Member of OSA and SPIE.

**Geert Morthier** (M'93–SM'01) received the M.Sc. degree in electrical engineering and the Ph.D. degree from Ghent University, Ghent, Belgium, in 1987 and 1991 respectively.

Since 1991, he has been a member of Interuniversity Microelectronics Center, Ghent University, Ghent, Belgium, and since 2001, he is a Part-time Professor at Ghent University. He is currently the Project Manager of the EU-HISTORIC project, which focuses on heterogeneously integrated microdisk lasers for gating and flip-flops and their combination into photonic integrated circuits. He has been involved in research on distributed feedback laser modeling, on widely tunable lasers and their control and on all-optical signal processing. He has authored or coauthored more than 150 papers in the field. He holds several patents. His current research interests include the modeling and characterization of optoelectronic and photonic components, and different types of all-optical flip-flops for optical packet switching.



**Pedro Rojo-Romeo** (M'09) was born in Madrid, Spain, in 1958. He received the InG.Dipl. degree in physics and the Ph.D. degree in electronic devices from the Institut National des Sciences Appliquées, Lyon, France, in 1981 and 1984, respectively.

Since 1988, he has been an Associate Professor in electronics at Institut des Nanotechnologies de Lyon, Ecole Centrale de Lyon, Lyon, where he is engaged in heterogeneous integration of III–V structures on Si-based substrates, development of CMOS compatible III–V nanolasers coupled to Si waveguides, develop-

ment of novel 2.5-D photonic crystal lasers for guided and free space laser emission, localization of nanostructures on a patterned surface using e-beam lithography techniques: localization of InAs quantum dots on InP for single photon sources, localized growth of III–V nanowires on Si, and localization of metal nanostructures for plasmonic applications. His current research interests include electrical and optical devices fabrication technology, characterization of microelectronic and optoelectronic micro- and nanodevices, optical interconnection systems, nanotechnologies, and optical integrated circuits technologies.

**Fabien Mandorlo** received the Engineer Diploma degree from the Ecole Centrale de Lyon, Lyon, France, the M.S. degree in electronics from the University of Lyon, Lyon, both in 2005, and the Ph.D. degree from both the Institute of Nanotechnologies of Lyon (INL), Lyon and the Commissariat à l'Energie Atomique/Laboratoire d'Electronique de Technologie de l'Information (CEA/LETI), Grenoble, France.

He is currently a Teaching Assistant at CEA/LETI. His research interests include microlasers and their integration in CMOS processes for optical integration in microelectronics.

**Philippe Regreny** was born in France, in 1967. He received the M.Sc. degree in materials science from Rennes University, Rennes, France, in 1991, and the Ph.D. degree in electronics from Ecole Centrale de Lyon, Lyon, France, in 1997.

Since 1998, he has been a Research Engineer at Institut des Nanotechnologies de Lyon (INL)/Center National de la Recherche Scientifique (CNRS), Ecole Centrale de Lyon. He has authored or coauthored 80 publications. His current research interests include epitaxial growth of III–V semiconductors and oxide materials and their integration on silicon.



**Oded Raz** (S'05–M'07) was born in the Netherlands, in 1970. He received the B.Sc. degree in electrical engineering from the Technion, Israel's Institute of Technology, Haifa, Israel, in 1993, and the M.Sc. and Ph.D. degrees from the Tel Aviv University, Tel Aviv, Israel, in 2002 and 2007, respectively.

Since 2007, he has been a Researcher at COBRA Research Institute, Technical University of Eindhoven, Eindhoven, The Netherlands, where he is currently an Assistant Professor. His research interests include all-optical signal processing for high-speed data signals, integrated III–V optical circuits, silicon-on-insulator (SOI) circuits, heterogeneous integration of InP over SOI for digital photonics, optical communications systems, and microwave photonics.



**Christophe Kopp** received the Ph.D. degree in photonic engineering from the University of Strasbourg, Alsace, France, in 2000.

In 2001, he has joined the Commissariat à l'Energie Atomique/Laboratoire d'Electronique de Technologie de l'Information (CEA/LETI), Grenoble, France, where he is engaged in developing assembling techniques for microoptoelectronic devices. His current research interests include high-speed optical data transmission applications, integrated silicon photonics design, and imaging systems.

**Laurent Grenouillet** received the Ing. Dipl. degree in physics, and the Ph.D. degree from the National Institute of Applied Sciences, Lyon, France, in 1998 and 2001, respectively.

He was a Postdoctoral Fellow in molecular beam epitaxy (MBE) at Commissariat à l'Energie Atomique/Laboratoire d'Electronique de Technologie de l'Information (CEA/LETI), Grenoble, France, where he joined the Optronics Department and was In-charge of the MBE growth of GaAs-based vertical cavity surface-emitting lasers emitting in the 1.1–1.3 $\mu$ m range and single photon sources. Since 2006, he has been involved in the field of silicon photonics. His current research interests include heterogeneous integration of III–Vs on silicon and CMOS compatible hybrid laser sources.